Intermetallics 17 (2009) 235–240

Contents lists available at ScienceDirect

Intermetallics

journal homepage: www.elsevier.com/locate/intermet

Biocompatibility of Ni-free Zr-based bulk metallic glasses

L. Liu [a,*], C.L. Qiu [a], C.Y. Huang [a], Y. Yu [a], H. Huang [b], S.M. Zhang [b]

[a] The State Key Laboratory of Die and Mould Technology, Huazhong University of Science and Technology, 430074 Wuhan, China
[b] Advanced Biomaterials and Tissue Engineering Center, Huazhong University of Science and Technology, 430074 Wuhan, China

ARTICLE INFO

Article history:
Received 31 May 2008
Received in revised form
28 July 2008
Accepted 28 July 2008
Available online 21 December 2008

Keywords:
B. biocompatibility
B. mechanical properties at ambient temperature
C. rapid solidification processing
D. microstructure

ABSTRACT

Three Ni-free Zr-based BMGs with composition of $Zr_{60}Nb_5Cu_{20}Fe_5Al_{10}$, $Zr_{60}Nb_5Cu_{22.5}Pd_5Al_{7.5}$, $Zr_{60}Ti_6Cu_{19}Fe_5Al_{10}$ were fabricated by suck copper-mould casting. All the BMGs prepared exhibit good glassy forming ability and wide supercooled liquid region ranging from 38 to 99 K. These BMGs also show good mechanical properties under static compression with yield strength of over 1350 MPa, Young's modulus of 70–80 GPa, and plastic strain of 3.6–9.5%. Friction and wear tests revealed that the BMGs exhibit much better wear resistance than the medical alloy Ti6Al4V, although BMGs have a higher friction coefficient. In addition, the *in vitro* test indicated that the BMGs have a similar or even better cell viability and proliferation activity as compared with Ti6Al4V. Finally, the *in vivo* evaluation of the BMGs was carried out by the implantation of BMG samples into white rabbits. It is shown that the BMG implants performed as well as the Ti alloy, demonstrating that the Ni-free Zr-based BMGs developed in this work are promising in medical applications.

1. Introduction

With the combination of superior strength, high elastic strain limit, relatively low Young's modulus, excellent corrosion resistance and wear resistance, Zr-based bulk metallic glasses show a promising potential for biomedical applications and have attracted much attention in recent years. Hiromoto et al. [1–4] investigated the effect of chloride-ion concentration, pH value, surface finishing and dissolved oxygen pressure on the polarization behavior of $Zr_{65}Cu_{17.5}Ni_{10}Al_{7.5}$ metallic glass in a phosphate buffered solution (PBS), and found that this amorphous alloy exhibited a similar polarization resistance to pure titanium. On the other hand, Horton and Parsell [5] carried out a series of tests on the biocompatibility of $Zr_{52.5}Al_{10}Ti_5Cu_{17.9}Ni_{14.6}$ BMG (BAM-11) through direct evaluation of the viability and metabolic activity of cells on the BMG surface. It was found that this BMG displayed as good biocompatibility as the titanium and polyethylene. Recently, Maruyama et al. [6] have performed a fretting fatigue study of an Zr-based amorphous alloy in PBS, and found that the fatigue strength can be as high as 150 MPa. However, most of the Zr-based BMGs for biocompatible study up to date contain the element Ni, which is usually blamed for the occurrence of allergy and is possibly carcinogenic to the human body [7,8]. To eliminate the negative effect of Ni, Jin and Löffler [9] have developed a series of Ni-free Zr-based BMGs; one of them, $Zr_{58}Cu_{22}Fe_8Al_{12}$ BMG, shows excellent glass forming ability and very good biocompatibility with the cell viability similar to Ti–6Al–4V alloy. The biocompatibility of this BMG can be further enhanced by a simple surface treatment of passivation with 30% HNO_3 due to the stabilization of Zr-oxide formed on the BMG surface, which blocks the dissolution of toxic ions [10]. However, the mechanical properties and corrosion resistance of the BMG are not adequately satisfactory.

Recently, we have successfully prepared a few new Ni-free Zr-based BMGs with a composition of $Zr_{60}Nb_5Cu_{20}Fe_5Al_{10}$, $Zr_{60}Nb_5Cu_{22.5}Pd_5Al_{7.5}$, and $Zr_{60}Ti_6Cu_{19}Fe_5Al_{10}$. In this paper, the mechanical properties, friction/wear behavior and the biocompatibility both *in vitro* and *in vivo* of these BMGs are systematically investigated. It will be shown that the BMGs exhibit good glass forming ability, excellent mechanical properties and very good biocompatibility.

2. Experimental

2.1. Sample preparation and structure characterization

Alloy ingots with nominal composition of $Zr_{60}Nb_5Cu_{20}Fe_5Al_{10}$, $Zr_{60}Nb_5Cu_{22.5}Pd_5Al_{7.5}$, and $Zr_{60}Ti_6Cu_{19}Fe_5Al_{10}$ were prepared from elemental metals (purity >99.5%) by arc melting under a Ti gettered Ar atmosphere. From the master alloys, a BMG rod of 3–5 mm diameter or a plate of 1.5 mm thickness was fabricated by copper-mould casting. The details of the fabrication process were reported elsewhere [11].

The amorphous feature of the as-cast BMGs (both the rod and plate) was verified by X-ray diffraction (XRD, χ′Pert PRO) with Cu

* Corresponding author. Tel.: +86 27 87556894; fax: +86 27 87554405.
E-mail address: lliu2000@mail.hust.edu.cn (L. Liu).

0966-9795/$ – see front matter © 2008 Elsevier Ltd. All rights reserved.
doi:10.1016/j.intermet.2008.07.022

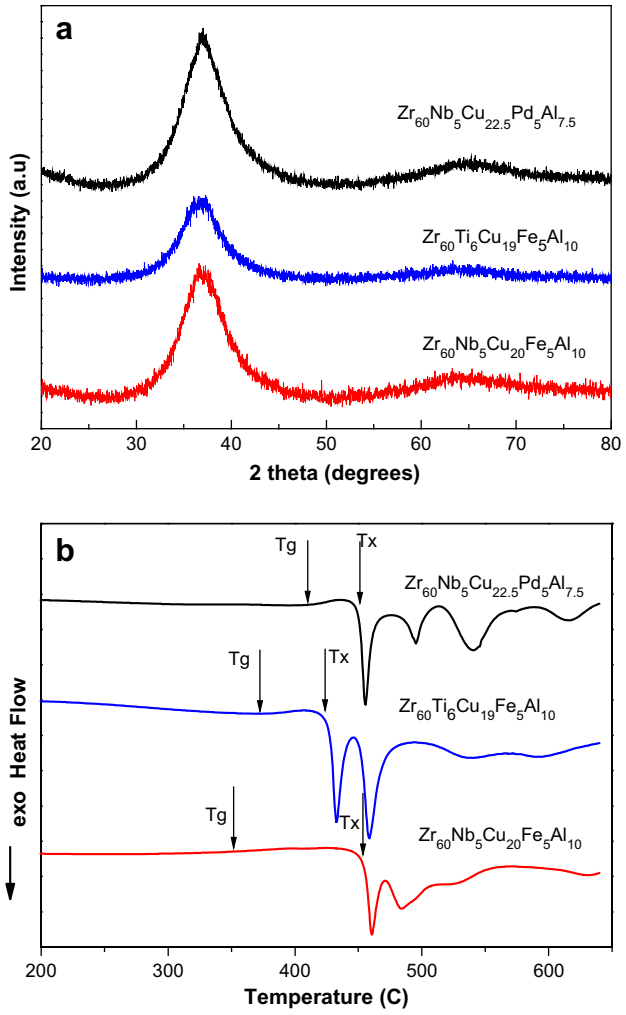

Fig. 1. The XRD patterns (a) and the DSC scans (b) of the three Ni-free Zr-based BMGs.

Kα radiation and transmission electron microscopy (TEM, JEM-2010). Glass transition and crystallization of the BMGs were examined using a differential scanning calorimetry (DSC, Perkin–Elmer 7) at a heating rate of 20 °C/min.

2.2. Mechanical properties and fraction/wear behavior

Mechanical properties of the BMG alloys were measured by using an MTS machine under compression at a strain rate of $1 \times 10^{-4}\,s^{-1}$. Samples with a length of 6 mm and diameter of 3 mm were cut from the rods for the tests. The fracture and lateral surfaces after compression were examined by scanning electron microcopy (SEM, Philips Quanta 200).

The friction/wear behaviors were investigated on an Optimol SRV oscillating friction and wear tester (German) in a ball-on-plate contact configuration. The upper ball in motion is made of zirconia with 10 mm diameter. The lower stationary plate is $Zr_{60}Ti_6Cu_{19}Fe_5Al_{10}$ BMG, cutting from the BMG plate, with a dimension of 5 mm × 10 mm × 1.5 mm. Ti–6Al–4V alloy with the same size was

Table 1
Thermodynamic data of the Ni-free Zr-based BMGs.

BMG systems	T_g	T_x	ΔT_x
$Zr_{60}Nb_5Cu_{22.5}Pd_5Al_{7.5}$	410	449	39
$Zr_{60}Ti_6Cu_{19}Fe_5Al_{10}$	372	426	54
$Zr_{60}Nb_5Cu_{20}Fe_5Al_{10}$	350	449	99

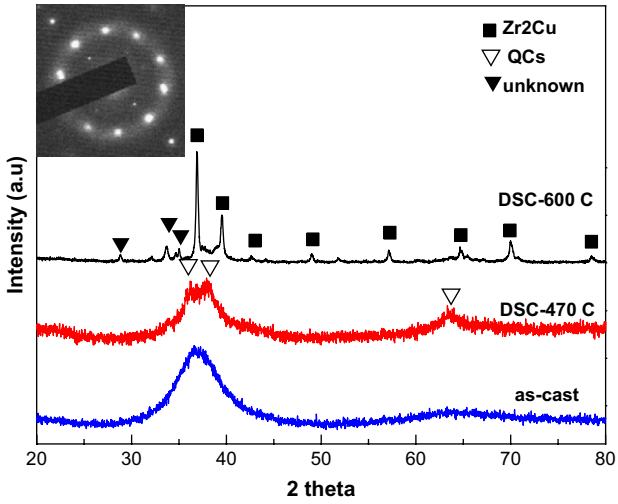

Fig. 2. The XRD patterns of $Zr_{60}Nb_5Cu_{20}Fe_5Al_{10}$ BMG after being annealed by *in situ* DSC scan to different temperatures, the inset is the electron diffraction pattern taken from a crystalline phase after the sample was scanned to 470 °C.

also tested for comparison. The friction test was performed in a horizontal oscillating mode with stroke length of 1.5 mm at a frequency of 10 Hz. The applied normal load and testing duration adopted in the study were 20 N and 300 s, respectively. Phosphate buffered solution (PBS) (with the composition of NaCl (8 g/L), KCl (0.2 g/L), $NaH_2PO_4 \cdot 2H_2O$ (0.14 g/L), KH_2PO_4 (0.20 g/L)) was used as a lubricator, which was carefully added such that the friction region was completely immersed. At least three tests were repeated for each alloy to ensure the data reproduction.

2.3. Examination of potential cytotoxicity of the BMGs

The potential cytotoxicity of the three BMGs was evaluated through cell culture for one week followed by 3-(4,5-dimethylthiazol-2-yl-)-2,5-diphenyltetrazolium bromide (MTT) assay (see Ref. [12] for the details of the MTT process). Three specimens for each BMG were tested simultaneously for dependability. The cytotoxicity of Ti–6Al–4V alloy was also evaluated under the same condition for comparison, and a blank test (i.e., cells were cultured in a standard 96 well plate without alloy samples) was taken as a control. The morphology of cells grown on the BMG samples was observed by SEM after cell culture.

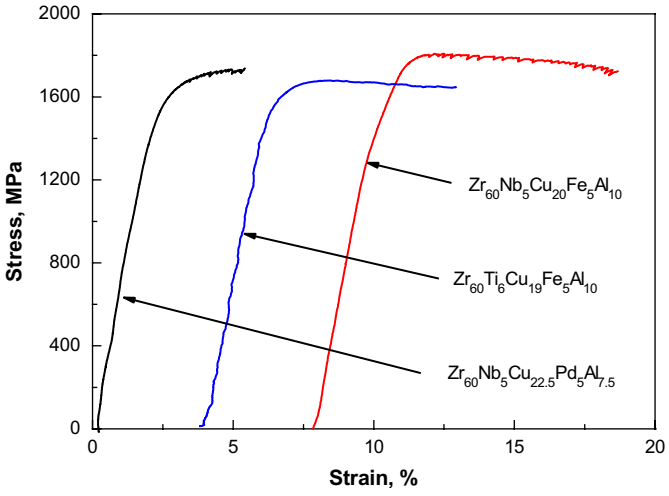

Fig. 3. Compressive stress–strain curves of the three Ni-free BMGs at a strain rate of $1 \times 10^{-4}\,s^{-1}$.

Table 2
Mechanical properties of the three Ni-free Zr-based BMGs.

Samples	σ_y, MPa	σ_f, MPa	E	ε_e, %	ε_p, %
$Zr_{60}Nb_5Cu_{22.5}Pd_5Al_{7.5}$	1378	1724	80	1.8	3.6
$Zr_{60}Ti_6Cu_{19}Fe_5Al_{10}$	1412	1652	70	2.0	7.0
$Zr_{60}Nb_5Cu_{20}Fe_5Al_{10}$	1393	1795	72	1.9	9.5

2.4. In vivo *evaluation of the BMGs*

For *in vivo* evaluation, one of the BMGs, $Zr_{60}Ti_6Cu_{19}Fe_5Al_{10}$, was chosen to implant into rabbits (in 3 groups) for 4–12 weeks. The medical alloy Ti–6Al–4V was also tested in the same condition for comparison. First, both BMG and Ti alloys were cut into pieces with a dimension of 3 mm × 3 mm × 1.5 mm from the BMG plate as implanting samples. Then, the samples were mechanically ground to 1200 grit and carefully sterilized according to the standard procedures. Both BMG and Ti–6Al–4V samples were simultaneously implanted in each rabbit at the central regions of the back through an anteromedial incision. After each 4 weeks, one of the animals was euthanized; the implants of BMG and Ti alloys were then taken out for SEM observation, while the surrounding tissues were carefully cut down for HE staining analysis.

3. Results and discussion

3.1. Structure and thermal stability

Fig. 1(a) shows the X-ray diffraction (XRD) patterns of the three alloys prepared. A broad diffraction hump without any trace of crystalline peaks in their XRD patterns indicates that the as-cast alloys are basically amorphous. The single amorphous structure of the alloys was further verified by TEM, which illustrated only a diffused diffraction ring in the electron diffraction pattern (not shown here). Fig. 1(b) shows the DSC curves of the three alloys at a heating rate of 20 °C/min. They all exhibit a distinct glass transition and a wide supercooled liquid region before crystallization. The glass transition temperature (T_g), the onset temperature of crystallization (T_x) and the resulting temperature interval of the

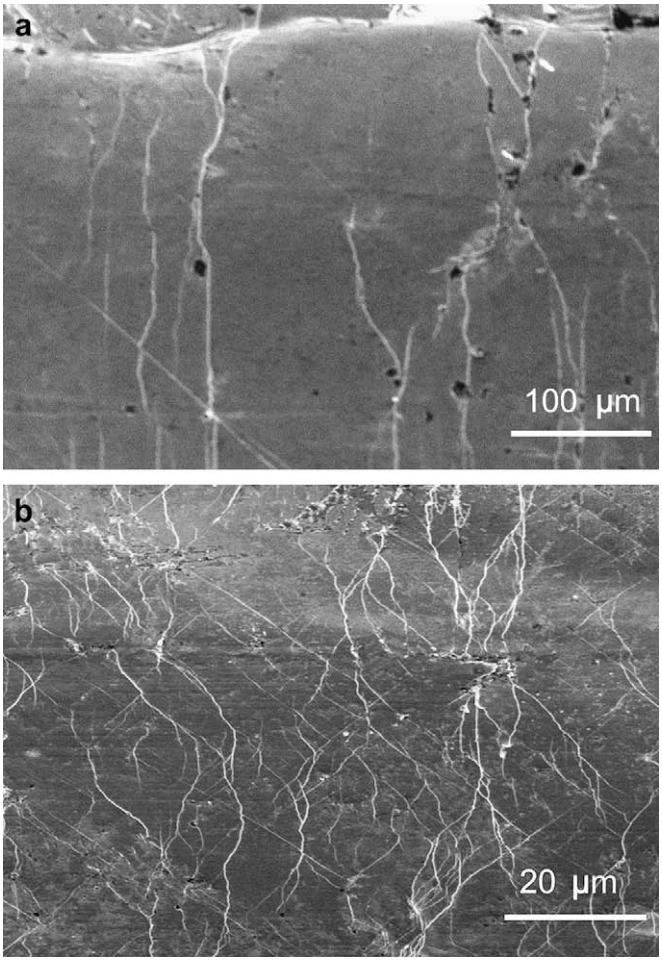

Fig. 4. SEM images of the lateral surfaces of $Zr_{60}Nb_5Cu_{22.5}Pd_5Al_{7.5}$ (a) and $Zr_{60}Ti_6Cu_{19}Fe_5Al_{10}$ (b) after compression to fracture.

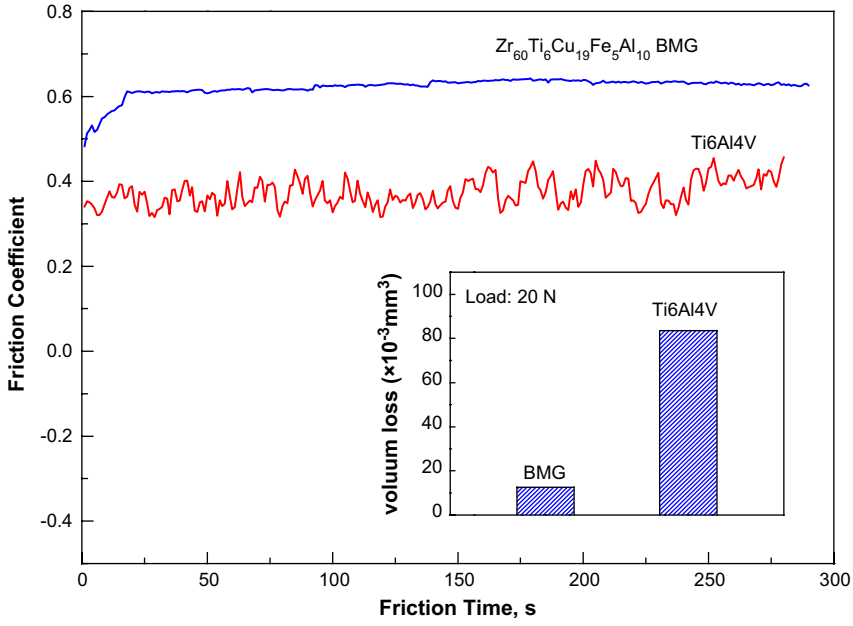

Fig. 5. The friction time dependence of the friction coefficient of $Zr_{60}Ti_6Cu_{19}Fe_5Al_{10}$ BMG and Ti–6Al–4V alloy. The inset is the comparison of volume loss between the BMG and Ti alloys after friction for 5 min.

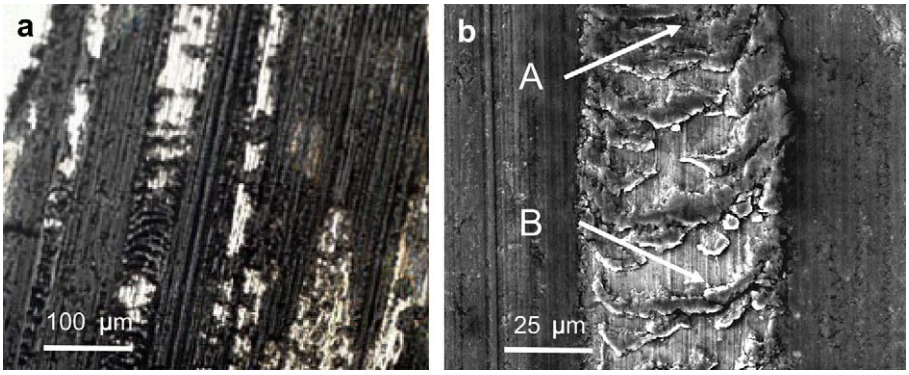

Fig. 6. (a) The overall morphology of the worn scar of $Zr_{60}Ti_6Cu_{19}Fe_5Al_{10}$ BMG at a low magnification; (b) the enlargement of a worn scar, indicating that a tribolayer was formed on the friction surface.

supercooled liquid region ($T_x = T_x - T_g$) are summarized in Table 1. The wide supercooled liquid region (i.e., from 38 K to 99 K) demonstrates that the three alloy systems in the study have excellent glass forming ability. It is also noted that all BMGs followed a multi-crystallization process under continuous heating. To clarify the phase transformation underlying various crystallization stages, the BMG samples that were heated, respectively, to various temperatures were examined by XRD. Fig. 2 shows the XRD patterns of $Zr_{60}Nb_5Cu_{20}Fe_5Al_{10}$ BMG, as an example, after being heated *in situ* by DSC to the end of the first peak (i.e., 470 °C) and the final stages (i.e., 600 °C). It can be seen that quasicrystals were preferentially formed in the first exothermic event, and finally transferred to a stable phase of Zr_2Cu after the completion of the crystallization process. The formation of quasicrystals of the BMG at the initial crystallization stage was further verified by TEM, which shows clearly a fivefold symmetry of the crystallized phase in its electron diffraction pattern (see the inset of Fig. 2). The other two BMGs follow the same phase transformation sequence, i.e., amorphous phase-quasicrystals-Zr_2Cu intermetallic compound. The preferential formation of quasicrystals implies that the amorphous phase of the BMGs may involve strong icosahedral short-range order clusters, which are believed to be beneficial for the enhancement of room-temperature plasticity.

3.2. Mechanical properties and friction/wear behavior

The stress–strain (σ–ε) curves of the three BMG samples under compressive loading at a strain rate of $1 \times 10^{-4}\,s^{-1}$ are shown in Fig. 3. The important mechanical properties, including yield strength (σ_y), fracture strength (σ_f), elastic strain (ε_e) and plastic strain (ε_p) measured from each of the σ–ε curves, are summarized in Table 2. It can be seen that all BMGs exhibit a high yield strength over 1300 MPa, and fracture strength over 1600 MPa. It is interesting to note that the three BMGs also exhibit a considerably large plastic strain, i.e., 3.6% for $Zr_{60}Nb_5Cu_{20}Fe_5Al_{10}$, 7.0% for $Zr_{60}Ti_6Cu_{19}Fe_5Al_{10}$, and 9.5% for $Zr_{60}Nb_5Cu_{22.5}Pd_5Al_{7.5}$, respectively, although they are apparently of a single amorphous structure on the basis of XRD and TEM results. In addition, the elastic strains around 2% with low modulus of 70–80 GPa were obtained. The modulus is lower than that of 316 L stainless steel (about 200 GPa) and Ti–6Al–4V alloy (110–125 GPa). To understand the plasticity of the BMGs under deformation, the lateral surface of the BMG samples after compression to fracture was further examined by SEM as shown in Fig. 4. It can be seen that a number of jagged and bifurcated shear bands distribute extensively on the surface of the compressed samples, and

Table 3
Composition (at%) of the tribolayer and the substrate of $Zr_{60}Ti_6Cu_{19}Fe_5Al_{10}$ BMG taken from regions A and B in Fig. 6(b).

Wear scar	Zr	Cu	Al	Fe	Ti	O
Tribofilm (Region A)	25.82	7.46	3.89	2.06	2.34	58.42
Substrate (Region B)	50.82	17.83	9.52	4.77	5.08	11.99

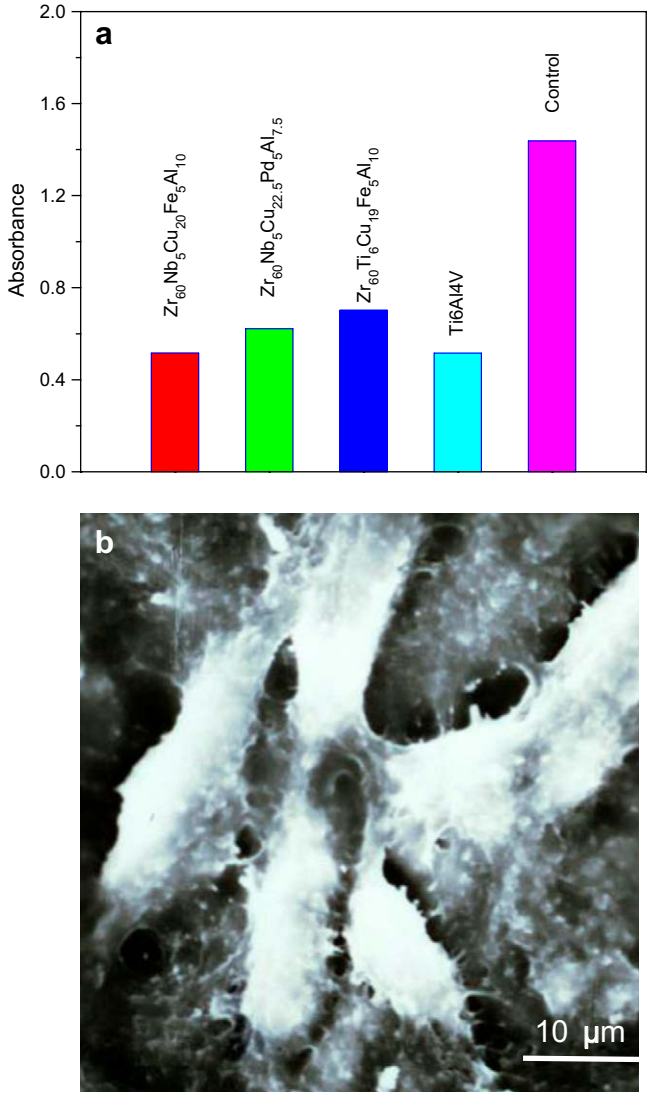

Fig. 7. (a) Cytotoxicity tests of the Ni-free Zr-based BMGs and Ti–6Al–4V alloy after cell culture for a week in comparison with the control; (b) The morphology of cells grown on the surface of $Zr_{60}Nb_5Cu_{20}Fe_5Al_{10}$ BMG after cell culture for a week.

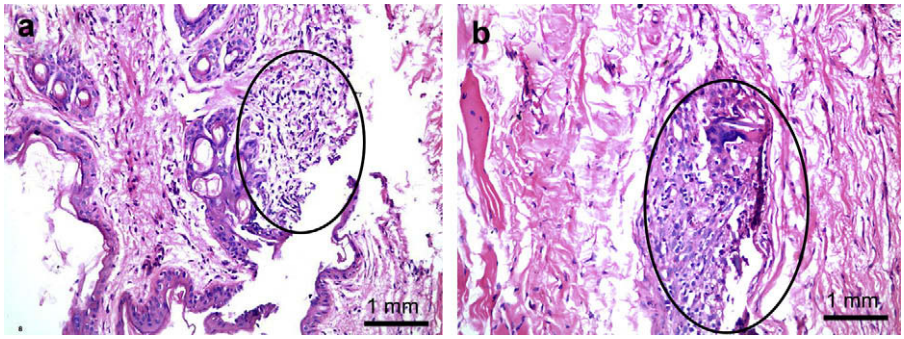

Fig. 8. The HE strained results of $Zr_{60}Ti_6Cu_{19}Fe_5Al_{10}$ BMG (a) and Ti–6Al–4V (b) after implantation for 12 weeks. The tissue in the circles was infiltrated with multinucleated giant cell and lymphocytes, which reflects the inflammatory reaction.

the density of shear bands is proportional to the plastic strain. This is consistent with the argument that the plasticity of BMG at room temperature phenomenally arises from shear banding.

A number of studies have been recently carried out to understand the origin of the room temperature plasticity of BMGs. It is generally believed that the existence of structural inhomogeneity, in the form of short/medium-range order clusters or phase separation, in amorphous phase contributes to the improvement of plasticity in monolithic BMGs [13–16], as the inhomogeneous structure can promote the generation of shear bands. This is also the case in the present study. In fact, the preferential precipitation of quasicrystals after annealing (see Fig. 2) implies that the icosahedral short/medium-range order structures have already existed in the as-cast BMGs. This structural inhomogeneity can induce the generation of multiple shear bands, and consequently lead to the enhancement of plasticity.

To investigate the friction and wear behavior of the BMGs, $Zr_{60}Ti_6Cu_{19}Fe_5Al_{10}$ BMG was chosen as an example and subjected to friction/wear test in phosphate buffered solution (PBS) under a load of 20N, and compared with Ti6Al4V medical alloy. Fig. 5 shows the friction curves of the BMG and Ti–6Al–4V. It can be seen that the friction of the BMG is relatively smooth as indicated by a very few variations in friction coefficient, while the friction of Ti6Al4V is characterized by large fluctuations. Obviously, the friction coefficient for BMG ($\sim$0.60) is much larger than that for Ti–6Al–4V ($\sim$0.35). The present results are not consistent with the arguments that BMGs should have a lower friction coefficient than crystalline materials. Similar results were also reported previously in other BMG alloys [17]. The inset in Fig. 5 shows the volume loss of the BMG and Ti6Al4V alloy after friction for 5 min. Compared with Ti alloy, the BMG exhibits much less volume loss, demonstrating that the BMG has a better wear resistance than Ti alloy although the former has a larger friction coefficient.

Fig. 6(a) shows the overall morphology of the worn scar of $Zr_{60}Ti_6Cu_{19}Fe_5Al_{10}$ BMG at low magnification. The worn surface is characterized by a series of fine wear grooves along the sliding direction. Fig.6(b) is the high magnification of one worn scar, from which one can see that a tribolayer with extensive distribution of micro-cracks was formed on the worn surface, and part of the tribolayer has already peeled out due to the propagation of the cracks. The composition of the tribolayer and the BMG substrate (as labeled as regions A and B in Fig.6(b)) was investigated by EDX and summarized in Table 3. It is found that the tribolayer contains a high concentration of oxygen. Considering that the elements of Zr, Al, Fe and Ti in the BMG have a strong affinity with oxygen, the tribolayer is most likely composed of the mixed metal oxides. Because of the brittleness of the oxides, the tribolayer is prone to crack and finally peel off during subsequent friction. Therefore, oxidation abrasion is believed to be the dominated wear mechanism of the BMG in phosphate buffered solution (PBS).

3.3. In vitro *and* in vivo *evaluation of the biocompatibility*

The *in vitro* evaluation of the biocompatibility of the BMGs was performed through cell culture followed by MTT assay. Fig. 7(a) shows the results of MTT assays for the three as-cast BMGs and Ti–6Al–4V after cell culture for 7 days. It can be seen that the BMGs show an absorbance similar to or even higher than that of Ti–6Al–4V alloy, implying that the BMG has high cell viability and proliferation activity. Fig. 7(b) shows the morphology of cells cultured on $Zr_{60}Nb_5Cu_{20}Fe_5Al_{10}$ BMG for 7 days. The cells closely adhered and well extended on the surfaces of the BMG, indicating that the Ni-free BMGs developed in this work exhibit an excellent biocompatibility.

Apart from the *in vitro* test, the biocompatibility of $Zr_{60}Ti_6Cu_{19}Fe_5Al_{10}$ BMG was also evaluated *in vivo* by implanting the BMG samples into white rabbits for a period of 4, 8 and 12 weeks. Ti–6Al–4V alloy with the same size was also implanted in the same rabbits for comparison. The *in vivo* tests revealed that a fibrous encapsulation with local infiltration was formed around both BMG and Ti–6Al–4V implants after 4 weeks, but no edema was observed in the two cases. However, the inflammatory response seems more serious for BMG than Ti alloy in the initial stage because the inflammation was only observed inside the fibrous capsule around Ti6–Al4–V, while it was also found outside the fibrous capsule around BMG. The inflammatory response was weakening gradually with the increase of the implanting time. After 12 weeks, both BMG and Ti alloy implants were completely encapsulated by mature fibrous connective tissue without any evidence of active proliferation. Fig. 8 shows the HE stained results of the tissue around BMG and Ti alloys after 12 weeks. It can be seen that slight inflammation still existed in the two cases, but the inflammatory reaction is only inside the fibrous capsule. The tissue was infiltrated predominantly with multinucleated giant cell and lymphocytes, as indicated by the circles shown in Fig. 8(a) and (b). No obvious difference in inflammation was observed between BMG and Ti–6Al–4V alloy after 12 weeks. These results indicate that the *in vivo* biocompatibility of BMG is as good as Ti–6Al–4V.

4. Conclusions

(1) Three new Ni-free Zr-based bulk metallic glasses were successfully fabricated by copper-mould casting. These BMGs show good glass forming ability and excellent mechanical properties with significant room-temperature plasticity.
(2) The Ni-free Zr-based BMGs demonstrate a much better wear resistance than the medical alloy Ti6Al4V in phosphate buffered solution (PBS) although the BMGs have even higher friction coefficient. The wear mechanism of the BMGs is dominated by oxidation abrasion.

(3) The Ni-free Zr-based BMGs show very good biocompatibility both *in vitro* and *in vivo*. The cytotoxicity and cell viability of the BMGs are similar to or better than Ti6Al4V alloy. The implanting test indicates that the BMGs perform as well as Ti6Al4V alloy, demonstrating that the Ni-free BMGs have promising potential in medical applications.

Acknowledgments

This work was financially supported by the Natural Science Foundation of China under grant No. 50571039 and 50871042. The authors are grateful to the Analytical and Testing Center, HUST for technical assistance.

References

[1] Hiromoto S, Tsai AP, Sumita M, Hanawa T. Corr Sci 2000;42:1651.
[2] Hiromoto S, Tsai AP, Sumita M, Hanawa T. Corr Sci 2000;42:2193.
[3] Hiromoto S, Tsai AP, Sumita M, Hanawa T. Corr Sci 2000;42:2167.
[4] Hiromoto S, Hanawa T. Electrochim Acta 2002;47:1343.
[5] Horton JA, Parsell DE. Mater Res Soc Symp Proc 2003;754:CC1.5.1.
[6] Maruyama N, Hiromoto S, Ohnuma M, Hanawa T. J Jpn Inst Met 2005;69:481.
[7] Uggowitzer J, Magdowski R, Speidel M. ISIJ Int 1996;36:901.
[8] Wataha JC, Lockwood PE, Schedle A. J Biomed Mater Res 2000;52:360.
[9] Jin K, Löffler JF. Appl Phys Lett 2005;85:241909.
[10] Buzzi S, Jin KF, Uggowitzer PJ, Tosatti S, Gerber I, Löffler JF. Intermetallics 2006;14:729.
[11] Liu L, Qiu CL, Chen Q, Chan KC, Zhang SM. J Biomed Mater Res A 2008;86:260.
[12] Qiu CL, Liu L, Sun M, Zhang SM. J Biomed Mater Res A 2005;75:950.
[13] Xing LQ, Li Y, Ramesh KT. Phys Rev B 2001;64:180211.
[14] Li J, Xu X, Hufnagel TC. Microsc Microanal 2003;9:509.
[15] Oh JC, Ohkubo T, Kim YC, Fleury E, Hono K. Scr Mater 2005;53:165.
[16] Park ES, Kyeong JS, Kim DH. Scr Mater 2007;57:49.
[17] Blau PJ. Wear 2001;250:431.